

Neutron Scattering Cross Sections of U^{233} , U^{235} , and Pu^{241} from 1 to 30 eV*

G. D. SAUTER

Department of Applied Science, University of California, Davis, California 95616

AND

C. D. BOWMAN

University of California, Lawrence Radiation Laboratory, Livermore, California 94550

(Received 23 May 1968)

Scattering cross sections for U^{233} , U^{235} , and Pu^{241} have been measured for neutron energies between 1 and 30 eV, using the 4π neutron source technique. For Pu^{241} , the scattering cross section and published fission data have been simultaneously fitted with Reich and Moore's multilevel formula. A good fit to both cross sections was obtained after allowing a sizable fluctuation in the resonance capture widths. Spin assignments were made for all observed resonances in the 2–32-eV interval. The average fission width for the $J=2$ levels is 510 MeV and for the $J=3$ levels is 190 MeV, in accordance with the spin-fission width correlation predicted by the Bohr-Wheeler theory.

EXPERIMENT

EPITHERMAL neutron scattering cross sections on U^{233} , U^{235} , and Pu^{241} have been measured at the Livermore electron linear accelerator. The measurements were carried out, using a 4π neutron source in a time-of-flight technique.¹ Our primary goal in making these measurements was to obtain total spin values J for as many resonances of U^{233} , U^{235} , and Pu^{241} as possible, and to confirm the prediction of Bohr² and Wheeler³ that for a given fissile isotope the total spin and average fission width are correlated. We have determined the scattering cross sections of U^{233} and U^{235} for neutron energies from 1 to 31 eV, and for Pu^{241} from 2 to 32 eV. In addition, total spin values have been assigned for all observed Pu^{241} resonances in the 2- to 32-eV interval. No spin assignments have been made for U^{233} or U^{235} .

The experimental arrangement is shown in Fig. 1. The principal feature of the 4π neutron source technique is the spherical carbon shell. When a pulse of high-energy (about 30-MeV) electrons strikes the tungsten target embedded in the shell, the resulting bremsstrahlung radiation creates a burst of high-energy neutrons via (γ, n) interactions with the tungsten. Some of these neutrons scatter back and forth in the moderating shell. After many successive scatters, these neutrons have slowed down to the energies of interest and have "forgotten" their point of origin and are uniformly distributed around the shell. Monte Carlo calculations have indicated that the inner surface of the moderating shell is a uniformly distributed 4π neutron source to within 5% for all neutron energies below 1 keV. For energies below 200 eV, the time t_0 (μ sec) after the elec-

tron pulse for maximum intensity of neutrons of energy E (eV) is $t_0 = 2.0/E^{1/2}$. The full width at half-maximum intensity τ (μ sec) is given by $\tau = 1.8/E^{1/2}$.

Neutrons from the inner surface of the shell are scattered by a thin sample placed in the center of the spherical cavity. Scattered neutrons emerging from the sample in the proper direction pass through a small hole in the shell and reach the boron-loaded liquid scintillator neutron detector. A second hole in the shell, diametrically opposite the first hole and backed by the "get lost" tube and a Li^6 absorber, prevents the detector from seeing any part of the carbon shell. Thus, the only direct neutron source seen by the detector is the scattering sample. Since the sample-to-detector flight time of fission neutrons and γ rays is much shorter than that of the scattered neutrons of interest, the background associated with fission and capture events is separated in time from the scattered neutrons.

The neutron detector used in these measurements consisted of a thin aluminum cup, 1.25 cm deep, fitted over the face of a 12.5-cm-diam EMI-9579B photo-multiplier tube and filled with boron-loaded liquid scintillator. The detector was used with a pulse-shape discrimination circuit¹ that rejected about 90% of those γ rays that gave rise to pulses from the scintillator with heights corresponding to those of slow neutrons, with a loss of about 25% in slow-neutron detection efficiency.

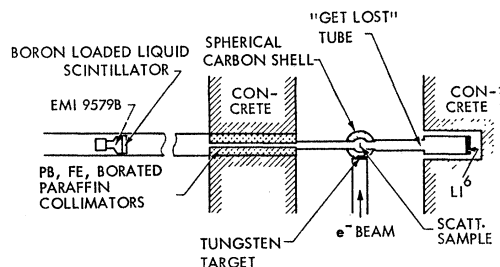


FIG. 1. Plan view of the experimental arrangement. The drawing is not to scale. The flight path length is 18.1 m.

* Work performed under the auspices of the U. S. Atomic Energy Commission.

¹ G. D. Sauter and C. D. Bowman, Nucl. Instr. Methods **55**, 141 (1967).

² A. Bohr, in *Proceedings of the Second United Nations International Conference on the Peaceful Uses of Atomic Energy, Geneva, 1958* (United Nations, Geneva, 1958).

³ J. A. Wheeler, Physica **22**, 1103 (1956).

For a thin scattering sample, it is shown in the Appendix that the neutron detection rate is proportional to the scattering cross section of the sample and the energy-dependent neutron flux incident on the sample. This flux can be determined from a measurement on a sample having a known scattering cross section, such as carbon. The two measurements can then be combined to yield the desired scattering cross section.

We made measurements on two samples of each of the fissile isotopes. With the exception of the thicker U^{238} sample, which was about 0.02 cm thick, all of the samples were less than 0.01 cm thick. Even for these relatively thin samples, it is necessary to make corrections for the reduction of the incident neutron flux due to neutron absorption before scattering occurs, and to take into account the possibility that a neutron scattered toward the detector will undergo a further reaction before leaving the sample. These corrections, which were not made to the data shown in Ref. 1, were most significant at the peaks of the large resonances. The largest correction was for the peak of the 2.31-eV resonance in the thicker U^{238} sample, where the corrected scattering cross section was a factor of 3.4 larger than the uncorrected value. In the valley regions between resonances, the corrections were generally less than 10%. The procedure for deducing the cross section from the data is described in the Appendix.

Plutonium-241

The two Pu^{241} -sample thicknesses were 1.14×10^{20} and 2.34×10^{20} atoms/cm². The isotopic composition of each sample was 0.8% Pu^{239} , 2.7% Pu^{240} , 85.7% Pu^{241} , 0.8% Pu^{242} , and 10.0% Am^{241} . When corrected for the effects of nonzero sample thickness, the two measurements yielded scattering cross sections which agreed very closely (to within 5% at the peaks of the largest reso-

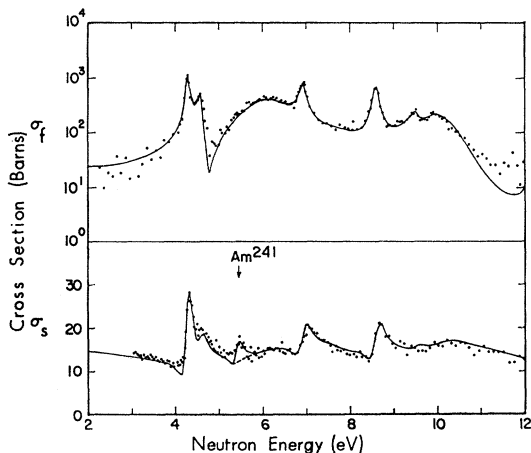


FIG. 2. The neutron scattering and fission cross sections of Pu^{241} from 2 to 12 eV. The solid curve is the simultaneous multi-level fit using the parameters of Table I.

nances). The resulting scattering cross section for Pu^{241} between 3 and 32 eV is shown in Figs. 2 and 3.

When the variation of the neutron scattering cross section with energy is known, attempts can be made to deduce the spins of the various resonance levels, using either area analysis or shape analysis. Area analysis, based on the single-level Breit-Wigner formula, has been successfully used in the case of Pu^{239} , where most of the resonances are sufficiently isolated from each other.⁴ For Pu^{241} , there appear to be only three levels for which area analysis is applicable; those at 13.38, 14.72, and 17.83 eV. We have area-analyzed our data for these three levels. The scattering area of an isolated resonance is given by $2\pi^2\lambda^2 g\Gamma_n^2/\Gamma$. From a measured scattering area, one can find $g\Gamma_n^2/\Gamma$. With this quantity and known values for $g\Gamma_n$ and Γ , the relation $g = [(g\Gamma_n)^2/\Gamma]/(g\Gamma_n^2/\Gamma)$ can be used to determine g . For the 13.38-, 14.72-, and 17.83-eV resonances, our data yield values for the scattering areas of 14.6, 29.9, and 18.2 b eV, respectively. Using published values⁵ for $g\Gamma_n$ and Γ , we then calculated g values of 0.36, 0.58, and 0.41, respectively. These indicate that the spins probably are $J=2$ ($g=0.417$) for the 13.38- and 17.83-eV levels and $J=3$ ($g=0.583$) for the 14.72-eV level.

We have also simultaneously fitted our Pu^{241} scattering data and the Pu^{241} fission cross section obtained by Moore *et al.*,⁶ using the multilevel cross-section formula of Reich and Moore⁷ with one fission channel per spin state and resolution and Doppler broadening included. This shape analysis is based on the following concept. Accurate values for $g\Gamma_n$ and Γ are known from earlier fission and total cross section measurements. The shape fit to the fission cross section is sensitive to the peak height and total width of the resonance, and thus actually determines the quantities $g\Gamma_n\Gamma_f/\Gamma^2$ and Γ . The peak cross section of a scattering resonance is proportional to $g\Gamma_n^2/\Gamma^2$. The shape fit to the scattering data, when combined with the total width determined from the fission fit, should yield a value of the product $g\Gamma_n^2$ that is independent of the value of spin assumed in the shape analysis, provided a good fit is obtained. (We will demonstrate this independence below.) With the value of $g\Gamma_n^2$ from our simultaneous shape fit and $g\Gamma_n$ from total data, the g value (and hence the spin) can be determined as $g = (g\Gamma_n)^2/(g\Gamma_n^2)$.

Assuming the spin values suggested by Moore *et al.*,⁶ we attempted to fit both scattering and fission cross section data, holding the capture width fixed and varying $g\Gamma_n\Gamma_f$, Γ and $g\Gamma_n^2$. However, we found that a satisfactory simultaneous fit could be obtained only by allowing a fluctuation in the capture width. The result-

⁴ G. D. Sauter and C. D. Bowman, Phys. Rev. Letters 15, 761 (1965); M. Asghar, Nucl. Phys. A98, 33 (1967).

⁵ J. R. Stehn *et al.*, Brookhaven National Laboratory Report No. 325 (U. S. Government Printing Office, Washington, D. C., 1958), 2nd ed., Suppl. 2, Vol. III.

⁶ M. S. Moore, O. D. Simpson, T. Watanabe, J. E. Russell, and R. W. Hockenbury, Phys. Rev. 135, B945 (1964).

⁷ C. W. Reich and M. S. Moore, Phys. Rev. 111, 929 (1958).

TABLE I. Resonance parameters for Pu^{241} .

E_0 (eV)	Γ_γ^a (meV)	Γ_n^a (meV)	Γ_f^a (meV)	$g\Gamma_n^b$ (meV)	^a	$g\Gamma_n^{2c}$ (meV) ²	^d	g^e	Assigned J
4.27	39	0.58	32+	0.33	0.195	0.195	0.216	0.56	3
4.57	25	0.47	142-	0.21	0.092	0.093	0.096	0.48	2
5.92	40	2.87	1330-	1.22	3.44	3.44	3.46	0.43	2
6.91	40	0.58	105-	0.35	0.196	0.196	0.194	0.62	3
8.57	30	0.61	85+	0.48	0.220	0.214	0.228	1.05	(3)
9.50	25	0.155	120-	0.092	0.014	0.016	0.016	0.61	3
10.20	35	1.85	990+	0.75	1.43	1.24	1.45	0.39	2
12.74	40	0.65	250-	0.39	0.248	0.240	0.241	0.62	3
13.39	57	3.15	36-	1.10	4.13	4.15	4.13	0.29	2
14.70	35	4.98	145+	3.07	14.5	15.6	13.8	0.65	3
15.98	40	1.32	475-	0.76	1.01	1.06	1.04	0.57	3
16.68	35	1.63	350+	0.61	1.12	0.930	0.950	0.33	2
17.86	80	4.35	37+	1.60	7.90	7.55	7.45	0.32	2
20.63	34	0.29	59+	0.17	0.048	0.042	0.048	0.61	3
22.88	60	1.10	335-	0.63	0.710	0.770	0.770	0.56	3
23.97	60	1.42	185+	0.79	1.18	1.10	1.22	0.54	3
26.30	30	3.60	315-	2.21	7.52	7.00	7.90	0.65	3
28.77	60	6.40	690+	2.42	17.1	18.4	15.1	0.34	2
29.33	35	0.49	70+	0.35	0.140	0.138	0.148	0.87	(3)
30.90	40	2.32	320+	1.44	3.15	3.18	3.46	0.65	3

^a Values obtained from final fit, using spins suggested by Moore *et al.* (Ref. 6) except for those resonances between 12.74 and 17.86 eV, where oppositer spins were used.

^b From Stehn *et al.* (Ref. 5).

^c Values obtained from the fit using spins suggested by Moore *et al.* (Ref. 6).

^d Values obtained from the fit using spins opposite those of Moore *et al.* (Ref. 6).

^e Computed from $g = (g\Gamma_n)^2 / (g\Gamma_n^2)$, using $g\Gamma_n^2$ values from final fit (Ref. a).

ing values for $g\Gamma_n^2$ are given in column 7 of Table I. For each resonance we then calculated g , using the published values⁵ for $g\Gamma_n$ that are listed in column 5 of Table I. The calculated g values were consistent with the initially assigned values except for the group of resonances between 12.78 and 17.83 eV. The spin for each of these resonances was opposite that suggested by Moore *et al.*⁶ Next we repeated the fitting process, assuming all spins opposite to those of Moore *et al.* For this fit, which yielded calculated cross sections that were nearly identical with those of the first fit, the computed values of $g\Gamma_n^2$ changed very little from those of the first fit. The values for $g\Gamma_n^2$ are given in column 8 of Table I. The g values determined in this case were again consistent with those proposed by Moore *et al.* except for the group of resonances between 12.78 and 17.83 eV. We therefore showed that the fits really were not sensitive to g but to the products $g\Gamma_n\Gamma_f$ and $g\Gamma_n^2$, which are related to the peak height in the fission and scattering data, respectively.

Finally, we carried out the fitting process for a third time using the spins suggested by Moore *et al.* for all resonances except those between 12.78 and 17.83 eV, for which the opposite values were used. Again the calculated cross sections were nearly identical with those of the previous fittings, and the computed values of $g\Gamma_n^2$, which are shown in column 6 of Table I, changed only slightly. The resulting g values, which are given in column 9 of Table I, were the same as those obtained from the two previous fits. Furthermore, the g values for the 13.38-, 14.72-, and 17.83-eV levels in all three fits were consistent with those determined by

area analysis as described earlier. The final parameters resulting from the fitting procedure for Pu^{241} are shown in the first four columns of Table I. Figures 2 and 3 show the experimental fission⁶ and scattering cross section data. The solid curves are the cross sections calculated from the multilevel formula using the resonance parameters listed in Table I.

The uniqueness of a multilevel fit has often been questioned owing to the large number (six) of parameters associated with each resonance. By requiring that two partial cross sections be fitted simultaneously, we believe that the uniqueness of the fit is significantly

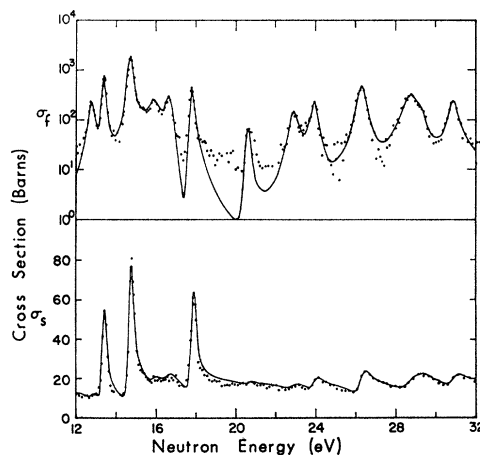


FIG. 3. The neutron scattering and fission cross sections of Pu^{241} from 12 to 32 eV. The solid curve is the simultaneous multilevel fit using the parameters of Table I.

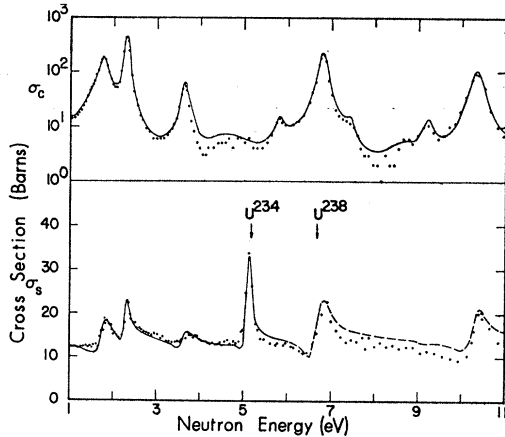


FIG. 4. The neutron scattering and capture cross sections of U^{238} from 1 to 11 eV. The solid and dashed lines are the multilevel fits described in the text.

strengthened. The possibility that levels with small neutron widths are missed also may weaken the validity of the multilevel fit. In fact, from a statistical analysis⁸ of resonance widths obtained from a multilevel fit to the fission cross section of Pu^{241} , at higher energies it is estimated that about 30% of the levels (those with small neutron widths) are missed. Since the scattering cross section is proportional to Γ_n^2 , this means that resonances with small Γ_n , which appear weakly in the fission cross section, will be entirely invisible in the scattering cross section since $\Gamma_n \ll \Gamma_f$ or Γ . Thus, the resonances with larger Γ_n that are observed in the scattering cross section are essentially undisturbed by the resonances with smaller Γ_n that are missed. The influence of missed resonances may be measured by the quality of the simultaneous fit to two partial cross

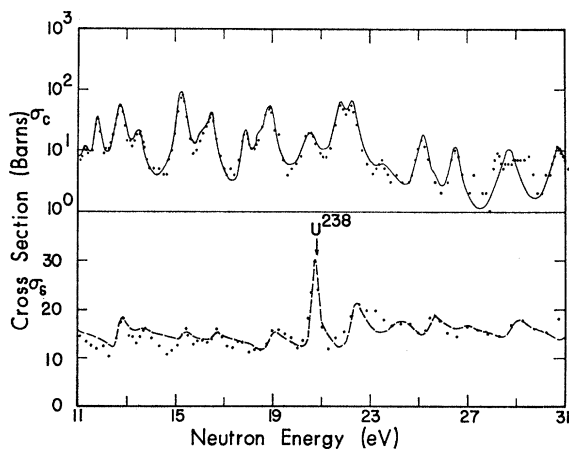


FIG. 5. The neutron scattering and capture cross sections of U^{238} from 11 to 31 eV. The solid and dashed lines are the multilevel fits described in the text.

⁸ O. D. Simpson, R. G. Fluharty, M. S. Moore, N. H. Marshall, B. G. Diven, and A. Hammendinger, in Proceedings of the Conference on Neutron Cross Section Technology, Washington, D. C., 1966 (unpublished).

sections and by the degree of scatter of g around the expected values of 0.417 and 0.583. Our values agree with the values suggested by Moore *et al.* for all levels except the group between 12.78 and 17.83 eV, where our values are opposite to theirs in every case.

Of the 20 levels considered here, we find 7 levels with $J=2$ and 13 levels with $J=3$. The average fission width of the $J=2$ levels is 510 meV and is 190 meV for the $J=3$ levels. These numbers are in excellent agreement with the average width 500 and 180 meV of the two groups found by Simpson⁸ on the basis of multilevel interference at higher energies. These values support the prediction of the Bohr-Wheeler theory^{2,3} that the $J=2$ levels should have a larger average fission width. Bohr and Wheeler⁹ have used the formula $2\pi(\Gamma_f/D)$, where D is the level spacing, to calculate the number of channels open for the fission process. For the $J=2$ and 3 states, the values are 0.77 and 0.55, respectively. Since a satisfactory fit to the fission cross section was obtained assuming one fission channel per spin state, these values can be interpreted as evidence that, for either spin state, one fission channel is at least half-way open.

TABLE II. Resonance parameters for U^{238} .

E_0 (eV)	Γ^a (meV)	$g\Gamma_n\Gamma_\gamma^a$ (meV) ²	$g\Gamma_n^2^b$ (meV) ²	$g\Gamma_n^c$ (meV)	$g\Gamma_n^d$ (meV)
1.59	645	3.9	0.0051	0.050	0.087
1.74	255	6.6	0.15	0.28	0.151
2.29	95	4.1	0.063	0.18	0.090
3.61	180	2.8	0.046	0.15	0.071
4.72	995	8.7	0.31	0.39	0.14
5.77	300	1.1			
6.77	210	28.1			
7.46	135	0.3			
8.67	745	4.7			
9.17	240	1.6			
10.30	280	33.1			
11.30	220	1.5			
11.81	200	6.9			
12.74	295	23.2			
13.54	345	9.2			
15.28	260	40.3			
16.14	395	14.5			
16.49	225	13.8			
17.91	160	2.9			
18.41	160	1.9			
18.90	325	43.0			
20.57	615	46.0			
21.81	225	25.2			
22.35	390	71.5			
23.62	945	31.6			
25.20	270	15.6			
25.72	75	0.2			
26.53	250	10.1			
28.76	505	31.1			
30.76	445	28.8			

^a Obtained from our fit to U^{238} capture data (Ref. 13).

^b Obtained from our fit to U^{238} scattering data.

^c Computed from the values in column 4 from the relationship

$g\Gamma_n \approx (0.5g\Gamma_n^2)^{1/2}$.

^d Taken from Ref. 5.

⁹ N. Bohr and J. A. Wheeler, Phys. Rev. **56**, 426 (1939).

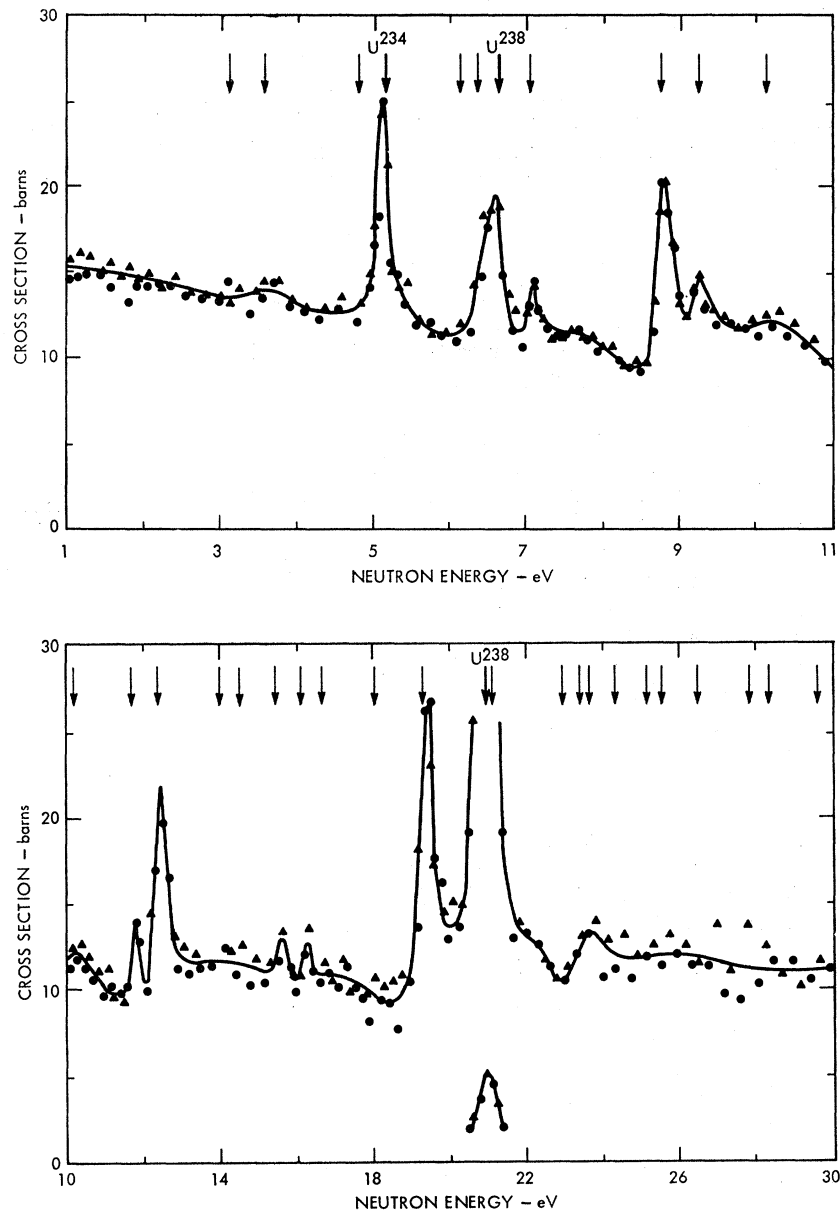


FIG. 6. The neutron scattering cross section of U^{235} from 1 to 31 eV. The solid line is included only to guide the eye. The dots and triangles represent the data from the thin and thick samples, respectively. The arrows indicate the positions of known resonances in U^{235} .

From the fluctuation in capture width we have used Willets's¹⁰ formula to obtain the number of exit channels γ_{eff} for the capture process. We find $\gamma_{\text{eff}} \approx 18$. There is no apparent correlation of capture width with the spin of the compound nucleus.

Uranium-233

The two U^{233} sample thicknesses were 4.83×10^{20} and 9.42×10^{20} atoms/cm². The isotopic composition of each sample was 97.3% U^{233} , 1.6% U^{234} , and 1.1% U^{238} , with trace amounts of other isotopes. For neutron energies above 15 eV, the data from the thicker sample were of

poor quality, because of the effects of the large γ flash created when each electron pulse was stopped by the tungsten target in the carbon shell. Thus for energies above 15 eV, only the thin sample data were used. For neutron energies below 15 eV, the two measurements, when corrected for the effects of sample thickness, again yielded scattering cross sections in good agreement. The measured neutron scattering cross section for U^{233} between 1 and 31 eV is shown by the data points in the lower section of Figs. 4 and 5.

The areas under scattering resonances in U^{233} appear to be too small, and the interference effects too large, to make area analysis feasible. We attempted a shape analysis by trying to simultaneously fit our scattering

¹⁰ L. Willets, Phys. Rev. Letters 18, 31 (1965).

data and the fission data of Nifenecker,¹¹ again using the multilevel formula of Reich and Moore with one fission channel per spin state. We could not obtain an acceptable simultaneous fit. Inasmuch as this same simultaneous fitting procedure was successful for Pu²⁴¹, this failure indicates that more than one fission channel per spin state is required to describe U²³³, in agreement with earlier work.¹²

We next attempted to derive a value for $g\Gamma_n^2$ by fitting, simultaneously, the capture data of Weston *et al.*¹³ and our scattering data. Since the capture process is associated with many exit channels for γ rays, no interference between resonances is expected. A single-level fit to the capture cross section will determine the total width Γ and the peak height, and hence the product $g\Gamma_n\Gamma_\gamma$. With the value of Γ thus determined, we attempted to fit the scattering data to obtain values for $g\Gamma_n^2$. The fit to the capture and scattering data is shown in the upper and lower sections of Figs. 4 and 5 by the line through the experimental points. The line through the scattering data is dashed above 6 eV since the fit above that energy is rather unsatisfactory. The parameters derived from this fitting procedure are given in the first four columns of Table II. As for Pu²⁴¹, we computed values of g for these levels from our values of $g\Gamma_n^2$ and the values of $g\Gamma_n$ obtained from other experiments.⁵ These computed g values were too far from the true values (0.583 or 0.417) to be meaningful. The discrepancy is related to a significant difference in our results for the neutron width in comparison with other measurements. We illustrate this by calculating approximate values of $g\Gamma_n$ from our data from the expression $g\Gamma_n \simeq (g\Gamma_n^2/2)^{1/2}$. These $g\Gamma_n$ values are shown in column 5 of Table II. Values from BNL-325⁵ are shown in column 6 of Table II. For the three prominent levels (1.74, 2.29, and 3.61 eV), our values for $g\Gamma_n$ are roughly a factor of 2 larger than those previously reported. If we assume that the BNL-325 values are correct, this result implies that our resonance scattering cross sections are a factor of 4 too high, since the peak height is proportional to the square of the neutron width. We believe that the accuracy of our data excludes this possibility. We have no explanation for the large difference between the two sets and conclude that reliable values for g can not be obtained from our scattering measurements on U²³³.

Uranium-235

The sample thicknesses used for the U²³⁵ measurements were 2.84×10^{20} and 4.18×10^{20} atoms/cm². The isotopic composition of each sample was 1.1% U²³⁴, 93.3% U²³⁵, and 5.6% U²³⁸. After corrections for effects

¹¹ H. Nifenecker, *J. Phys. (Paris)* **25**, 877 (1964).

¹² For example, M. S. Moore and C. W. Reich, *Phys. Rev.* **118**, 718 (1960); E. Vogt, *ibid.* **118**, 724 (1960).

¹³ L. W. Weston, R. Gwin, G. deSaussure, R. W. Ingle, R. R. Fullwood, and R. W. Hockenbury, Oak Ridge National Laboratory Report No. ORNL-TM-1751, 1967 (unpublished).

of sample thickness, the scattering cross sections determined from the two measurements are in satisfactory agreement. The resulting scattering cross section for U²³⁵ between 1 and 31 eV is shown in Fig. 6 for each sample thickness. The arrows in the figure indicate the positions of known resonances in U²³⁵. Because of the complex resonance structure of U²³⁵, we have not attempted any area or shape analysis of this data.

CONCLUSIONS

From our measurements on U²³³, U²³⁵, and Pu²⁴¹, we have determined the neutron scattering cross sections for these nuclides for neutron energies below 31 eV. For Pu²⁴¹, we have deduced the spins of 20 levels between 2 and 32 eV and confirmed the correlation between average fission width and resonance spin predicted by the Bohr-Wheeler theory. Although no spin assignments could be made for U²³³, we have obtained provisional values for Γ and $g\Gamma_n\Gamma_\gamma$ for the resonances between 1 and 31 eV.

ACKNOWLEDGMENTS

We gratefully acknowledge the help of G. F. Auchampaugh, who supplied the multilevel code used in the analysis, the support of the National Science Foundation and the Control Data Corporation in providing the digital computer facilities and the encouragement of Professor H. Mark in this work.

APPENDIX: EXTRACTION OF CROSS SECTIONS INCLUDING EFFECTS OF FINITE SAMPLE THICKNESS

As previously pointed out in this paper, the effects of nonzero sample thickness on the scattering data obtained using the 4π source technique are significant even for samples less than 0.01 cm thick. In analyzing the data, consideration must be given to such processes as depression within the sample of the incident neutron flux, and further reactions in the sample after neutrons have scattered in it. This Appendix outlines a method of determining the scattering cross section from the measurements, which is shown to be accurate to a few percent.

Consider the geometry of Fig. 7 for a scattering sample of thickness n atoms/cm². Let the strength of the 4π neutron source (the inner surface of the graphite shell) be $I_0(E_1)$ neutrons/cm² sec eV. $I_0(E_1)$ is spatially independent but varies smoothly and slowly with energy. Further, let δ be the area of each of the two small holes in the source, and let Ω be the solid angle subtended by the neutron detector. The effective area of the sample is the area A seen by the detector through the collimation. As a first approximation, assume that the absorption cross section of the sample is negligible

and that no neutron is scattered more than once in the sample.

A surface element da of the source emits $I_0(E_1)da$ neutrons sec eV, of which $I_0(E_1)[A\mu/4\pi r^2]da$ reach the effective region of the sample, where $\mu = \cos\theta$. Assuming isotropic scattering (a good assumption for low-energy neutrons and heavy scattering nuclei), the probability for any such neutron to be scattered into the solid angle Ω is $\sigma_s(E_1)[n\Omega/4\pi\mu]$, where $\sigma_s(E_1)$ is the scattering cross section of the sample for neutrons of energy E_1 . Thus, the rate per unit energy at which neutrons of energy E_1 from da are scattered and reach the detector is $I_0(E_1)\sigma_s(E_1)[nA\Omega/16\pi^2 r^2]da$. Integrating over the area of the source, the total rate per unit energy at which source neutrons of energy E_1 are scattered and reach the detector is $I_0(E_1)\sigma_s(E_1)nA\Omega[(4\pi r^2 - 2\delta)/16\pi^2 r^2]$.

If the thermal motion of the scattering nuclei is neglected, the scattered neutrons which left the source at energy E_1 will reach the detector with energies between E_1 and αE_1 , where $\alpha \equiv (M-1)^2/(M+1)^2$, M being the mass number of the scattering nuclei. This spread in energy, which results from variation of energy loss upon scattering with scattering angle, is about 2% for fissile nuclei. In the time-of-flight technique used here, the measured neutron energy, which characterizes the detector response, is the energy of the scattered neutrons. If the scattered neutron energy is E_2 , the detector response at E_2 will be due to neutrons that left the source with energies E_1 between E_2/α and E_2 , the average energy E_1 being $\bar{E}_1 = 2E_2/(1+\alpha)$. Thus, the rate per unit energy at which scattered neutrons of energy E_2 are detected can be closely approximated by

$$R(E_2) = I_0(\bar{E}_1)\sigma_s(\bar{E}_1)\epsilon(E_2)nA\Omega \times [(4\pi r^2 - 2\delta)/16\pi^2 r^2], \quad (A1)$$

where $\epsilon(E_2)$ is the detector efficiency at energy E_2 .

The thermal motion of the scattering nuclei increases the spread of source energies which contribute to the detector response $R(E_2)$ and slightly reduces the value of \bar{E}_1 for a given E_2 . Neither of these effects is significant here. The resolution of these measurements, which is affected by both the thermal motion of the nuclei and the variation of energy loss upon scattering with scattering angle, has been previously described.¹

The desired scattering cross section can be determined from Eq. (A1) if the neutron source strength $I_0(\bar{E}_1)$ is known. This quantity can be determined from a measurement with a scattering sample for which the scattering cross section is known and the absorption cross section is negligible. It is particularly convenient to pick a sample, such as carbon or aluminum, for which the cross section is energy-independent in the region of interest. Let such a sample be of thickness n_l and have an energy-independent scattering cross section σ_l such that $n_l\sigma_l \ll 1$. Then, with $E_3 = (1+\alpha)\bar{E}_1/2$,

$$R_l(E_3) = I_0(\bar{E}_1)\sigma_l\epsilon(E_3)n_lA\Omega[(4\pi r^2 - 2\delta)/16\pi^2 r^2] \quad (A2)$$

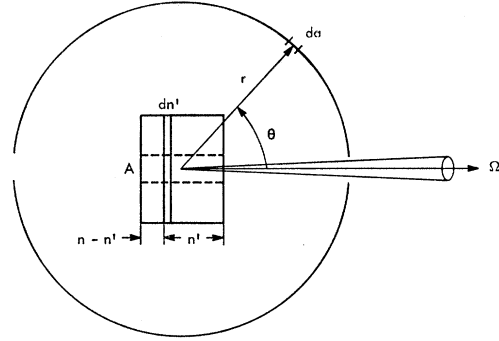


FIG. 7. The geometry of the 4π neutron source technique. Neutrons from element da of the spherical source are scattered by the element dn' of the sample into the solid angle Ω subtended by the detector. The dashed lines indicate A , the effective area of the sample seen through collimators by the detector. The sample thickness is n atoms/cm². $\cos\theta \equiv \mu$.

is the detection rate per unit energy for scattered neutrons of energy E_3 . Combining Eqs. (A1) and (A2) then yields

$$\sigma_s(\bar{E}_1) = \frac{R(E_2)}{R_l(E_3)} \frac{n_l\sigma_l}{n} \frac{\epsilon(E_3)}{\epsilon(E_2)}, \quad (A3)$$

where $E_2 = \frac{1}{2}(1+\alpha)\bar{E}_1$, and $E_3 = \frac{1}{2}(1+\alpha)\bar{E}_1$. For our detector, $\epsilon(E_3)/\epsilon(E_2) \approx 1$.

The scattering cross section $\sigma_s(\bar{E}_1)$ given by Eq. (A3) is the cross section one would obtain if absorption and multiple scattering in the sample are neglected. This neglect is reasonable in the spectrum sample, where $n_l\sigma_l \ll 1$. However, in the region of a resonance in the fissile sample generally $n\sigma_s \ll n\sigma_a \approx 0.1$, so that the effects of neutron absorption and multiple scattering must be considered. Equation (A3) can be used to calculate $\sigma_s(\bar{E}_1)$ if $R(E_2)$ is computed more accurately than in Eq. (A1). In recalculating $R(E_2)$, the value δ , which does not affect the result for $\sigma_s(\bar{E}_1)$, will be assumed to be zero.

Again referring to Fig. 7, for $0 < \theta < \frac{1}{2}\pi$, the rate per unit energy at which source neutrons of energy E_1 from da reach the effective area A of the sample element dn' is

$$I_0(E_1)[A\mu/4\pi r^2]e^{-n'\sigma(E_1)/\mu}da,$$

where $\sigma(E_1)$ is the total cross section of the sample. The probability that such a neutron is scattered in the element dn' into the solid angle Ω and leaves the sample without further reaction is

$$\sigma_s(E_1)[\Omega dn'/4\pi\mu]e^{-\sigma_2(E_1)n'}.$$

Thus, the rate per unit energy at which source neutrons of energy E_1 from da are scattered in dn' and reach the detector is

$$I_0(E_1)\sigma_s(E_1)[A\Omega/16\pi^2 r^2] \times \exp\{-n'[\sigma(E_2) + \sigma(E_1)/\mu]\}da dn'.$$

For the region $\frac{1}{2}\pi < \theta < \pi$, we can get a similar result by replacing $e^{-n'\sigma(E_1)/\mu}$ by $e^{-(n-n')\sigma(E_1)/\mu}$ and again letting $0 < \mu < 1$. It should be noted that we have neglected any neutrons that reach the detector after more than one scattering in the sample. This multiple-scattering contribution will be very small for samples where $n\sigma_s \ll 1$, such as was the case in our measurements. Letting $da = 2\pi r^2 d\mu$, the rate per unit energy at which scattered neutrons of energy E_2 are detected is

$$R(E_2) = \epsilon(E_2) [A\Omega/8\pi] \int_0^n \int_0^1 I_0(E_1) \sigma_s(E_1) \times e^{-n'\sigma(E_2)} [e^{-n'\sigma(E_1)/\mu} + e^{-(n-n')\sigma(E_1)/\mu}] d\mu dn'. \quad (\text{A4})$$

The energy E_1 , for a given value of E_2 , will be a function of μ .

If the thermal motion of the sample nuclei is again neglected, an approximate evaluation of $R(E_2)$ can be made by again assuming that a single energy \bar{E}_1 , independent of the scattering angle, can be used to characterize all the incident neutrons. A reasonable value of \bar{E}_1 is again $E_2 = \frac{1}{2}(1+\alpha)\bar{E}_1$. For convenience, let $\sigma(\bar{E}_1) \equiv \sigma_1$ and $\sigma(E_2) \equiv \sigma_2$. The integrations can now be carried out in a lengthy but straightforward manner, using the well-known functions

$$E_1(x) \equiv \int_x^\infty \frac{1}{t} e^{-t} dt \quad \text{and} \quad \bar{E}_1(x) \equiv \int_{-\infty}^x \frac{1}{t} e^t dt$$

and their series expansions for small x :

$$E_1(x) \approx -\ln(1.7811x) + x - \frac{x^2}{2 \times 2!} + \frac{x^3}{3 \times 3!} + \dots,$$

$$\bar{E}_1(x) \approx \ln(1.7811x) + x + \frac{x^2}{2 \times 2!} + \frac{x^3}{3 \times 3!} + \dots.$$

The results are

$$R(E_2) = I_0(\bar{E}_1) \epsilon(E_2) [A\Omega/8\pi] \times [\sigma_s(\bar{E}_1)\sigma_2] f_1(n, \sigma_1, \sigma_2), \quad \text{if } \sigma_1 > \sigma_2 \quad (\text{A5a})$$

and

$$R(E_2) = I_0(\bar{E}_1) \epsilon(E_2) [A\Omega/8\pi] \times [\sigma_s(\bar{E}_1)/\sigma_2] f_2(n, \sigma_1, \sigma_2), \quad \text{if } \sigma_1 < \sigma_2 \quad (\text{A5b})$$

where

$$f_1(n, \sigma_1, \sigma_2) \equiv 1 - e^{-n\sigma_1(1+\sigma_2/\sigma_1)} - e^{-n\sigma_2} [1 - e^{-n\sigma_1(1-\sigma_2/\sigma_1)}] - (\sigma_1/\sigma_2) \{ E_1[n\sigma_1(1+\sigma_2/\sigma_1)] + E_1[n\sigma_1(1-\sigma_2/\sigma_1)] e^{-n\sigma_2} + \ln(1+\sigma_2/\sigma_1) + \ln(1-\sigma_2/\sigma_1) e^{-n\sigma_2} \} + E_1(n\sigma_1) [(\sigma_1/\sigma_2 + n\sigma_1) e^{-n\sigma_2} + (\sigma_1/\sigma_2 - n\sigma_1)], \quad (\text{A6a})$$

and

$$f_2(n, \sigma_1, \sigma_2) \equiv 1 - e^{-n\sigma_1(1+\sigma_2/\sigma_1)} + e^{-n\sigma_2} [e^{n\sigma_1(\sigma_2/\sigma_1-1)} - 1] - (\sigma_1/\sigma_2) \{ E_1[n\sigma_1(1+\sigma_2/\sigma_1)] - \bar{E}_1[n\sigma_1(\sigma_2/\sigma_1-1)] e^{-n\sigma_2} + \ln(1+\sigma_2/\sigma_1) + \ln(\sigma_2/\sigma_1-1) e^{-n\sigma_2} \} + E_1(n\sigma_1) [(\sigma_1/\sigma_2 + n\sigma_1) e^{-n\sigma_2} + (\sigma_1/\sigma_2 - n\sigma_1)]. \quad (\text{A6b})$$

$I_0(\bar{E}_1)$ can be determined from Eq. (A2) as before, this time with $\delta=0$. Then $\sigma_s(\bar{E}_1)$ can be determined from Eqs. (A5a) and (A5b) as

$$\sigma_s(\bar{E}_1) = \frac{R(E_2) \epsilon(E_2) n_1 \sigma_1}{R_1(E_2) \epsilon(E_2) n} \frac{2n\sigma_2}{f_1(n, \sigma_1, \sigma_2)}, \quad \text{if } \sigma_1 > \sigma_2 \quad (\text{A7a})$$

and

$$\sigma_s(\bar{E}_1) = \frac{R(E_2) \epsilon(E_2) n_1 \sigma_1}{R_1(E_2) \epsilon(E_2) n} \frac{2n\sigma_2}{f_2(n, \sigma_1, \sigma_2)}, \quad \text{if } \sigma_1 < \sigma_2. \quad (\text{A7b})$$

A more precise approximation to the integral over μ in Eq. (A4) can be made by dividing the spherical-shell neutron source into many intervals with respect to μ and evaluating $\sigma(E_1)$ at the average incident energy in each interval for a given scattered neutron energy E_2 . The neutron-source spectrum $I_0(E_1)$ varies slowly with E_1 , so it can still be adequately represented by $I_0(\bar{E}_1)$ as given by Eq. (A2). The scattering cross section is again assumed to be $\sigma_s(\bar{E}_1)$. The resulting form of the equation for $\sigma_s(\bar{E}_1)$ is the same as that of Eqs. (A7a) and (A7b), but the factors f_1 and f_2 are considerably more complicated than shown in Eqs. (A6a) and (A6b).

Using published values for total cross sections,⁵ we have evaluated $\sigma_s(\bar{E}_1)$ for Pu²⁴¹ between 12 and 20 eV, both by using Eqs. (A7a) and (A7b) and by the method outlined in the preceding paragraph with twenty equal intervals comprising the source. The agreement between the two methods was very good, the resulting cross sections agreeing in every instance to within 1%. The remaining data for Pu²⁴¹ and all the data for U²³³ and U²³⁵ were analyzed using Eqs. (A7a) and (A7b).